Strength and deformation of shocked diamond single crystals: Orientation dependence

J. M. Lang,* J. M. Winey, and Y. M. Gupta
Institute for Shock Physics and Department of Physics and Astronomy, Washington State University, Pullman, Washington 99164, USA

(Received 19 September 2017; revised manuscript received 8 January 2018; published 19 March 2018)

Understanding and quantifying the strength or elastic limit of diamond single crystals is of considerable scientific and technological importance, and has been a subject of long standing theoretical and experimental interest. To examine the effect of crystalline anisotropy on strength and deformation of shocked diamond single crystals, plate impact experiments were conducted to measure wave profiles at various elastic impact stresses up to ∼120 GPa along [110] and [111] crystal orientations. Using laser interferometry, particle velocity histories and shock velocities in the diamond samples were measured and were compared with similar measurements published previously for shock compression along the [100] direction. Wave profiles for all three orientations showed large elastic wave amplitudes followed by time-dependent inelastic deformation. From the measured wave profiles, the elastic limits were determined under well characterized uniaxial strain loading conditions. The measured elastic wave amplitudes for the [110] and [111] orientations were lower for higher elastic impact stress (stress attained for an elastic diamond response), consistent with the result reported previously for [100] diamond. The maximum resolved shear stress (MRSS) on the $\{111\}\langle 110\rangle$ slip systems was determined for each orientation, revealing significant orientation dependence. The MRSS values for the [100] and [110] orientations (∼33 GPa) are 25%–30% of theoretical estimates; the MRSS value for the [111] orientation is significantly lower (∼23 GPa). Our results demonstrate that the MRSS depends strongly on the stress component normal to the $\{111\}$ planes or the resolved normal stress (RNS), suggesting that the RNS plays a key role in inhibiting the onset of inelastic deformation. Lower elastic wave amplitudes at higher peak stress and the effect of the RNS are inconsistent with typical dislocation slip mechanisms of inelastic deformation, suggesting instead an inelastic response characteristic of shocked brittle solids. The present results show that the elastic limit (or material strength) of diamond single crystals cannot be described using traditional isotropic approaches, and typical plasticity models cannot be used to describe the inelastic deformation of diamond. Analysis of the measured wave profiles beyond the elastic limit, including characterization of the peak state, requires numerical simulations that incorporate a time-dependent, anisotropic, inelastic deformation response. Development of such a material description for diamond is an important need.

DOI: 10.1103/PhysRevB.97.104106

I. INTRODUCTION

Due to its exceptional mechanical, optical, and thermal properties, diamond has attracted strong interest both scientifically and technologically [1]. Regarding its mechanical properties, the focus of the present study, quantifying and understanding the shear strength or elastic limit of diamond single crystals is of fundamental scientific interest, and considerable efforts have been made to achieve theoretical estimates of its shear strength [2–9]. However, experimental determination of diamond shear strength has remained a significant challenge.

Regarding theoretical estimates of the diamond shear strength reported in the literature [2–9], we point out that accurate knowledge of the third-order elastic constants is an important and essential step toward strength determination for a strong cubic crystal like diamond. Because experimental and theoretical issues regarding the third-order elastic constants of diamond have been resolved only recently [10,11], previous theoretical estimates of diamond shear strength need to be examined carefully.

Due to the extremely high strength and stiffness of diamond, and the need for accurately quantifying the imposed stress state, precise strength determination using conventional quasistatic loading approaches is difficult. Thus, the determination of the elastic limit of diamond single crystals remains an important scientific challenge. In this paper, the terms shear strength and elastic limit are used interchangeably, depending on the specific context.

Plate impact experiments, resulting in plane shock wave compression, provide an excellent approach to measure the elastic limit of diamond single crystals under well-characterized loading conditions. Although these experiments require special facilities and are expensive, the uniaxial strain compression imparted to the samples in these experiments can be quantified precisely. This feature avoids the stress state limitations inherent in quasistatic loading. Furthermore, this approach is optimally suited to determine and compare the elastic limits for diamond crystals shock compressed along different crystallographic directions. Plane shock wave profile measurements from plate impact experiments and their analysis constitute the conceptual basis for the results reported in this paper.

*Present address: Shock and Detonation Physics Group, Los Alamos National Laboratory, Los Alamos, NM 87545.

Early shock wave studies to examine diamond strength were quite limited, consisting of exploratory efforts [12,13] that yielded somewhat ambiguous results [12]. Recently, Lang and Gupta used plate impact experiments to measure wave profiles for natural and synthetic type IIa diamond single crystals shock compressed along the [100] direction to ∼90 and ∼120 GPa elastic impact stresses (EIS). [14] The EIS—the longitudinal stress attained for a purely elastic response—can be determined accurately in plate impact experiments and provides a well-defined initial condition for ensuring consistent comparisons between experiments along different crystal orientations and at different stress inputs.

For both natural and synthetic single crystals, the measured wave profiles in Ref. [14] showed elastic-inelastic response with a maximum elastic wave amplitude of ∼90 GPa and strongly time-dependent inelastic deformation response beyond the elastic limit. Surprisingly, the elastic wave amplitude for the ∼120 GPa (EIS) was lower than the ∼90 GPa (EIS). This result is discussed later in this paper.

The work reported here builds on our previous study [14], and was motivated by the goal to examine and understand anisotropy effects in shock compressed diamond single crystals. Shock wave studies on other single crystals have demonstrated that strength and deformation can display significant anisotropy [15–17]. Hence, a comprehensive understanding of the diamond elastic limit and deformation requires experimental measurements along different crystal orientations. Specifically, we wanted to address the following issues: (1) Does the elastic-inelastic response of diamond single crystals show significant orientation dependence? (2) How to understand the observed orientation dependence of the measured elastic limit in shocked diamond single crystals? (3) Will other orientations also display the lower elastic limit observed [14] for the [100] orientation at the higher elastic impact stress (EIS)?

To address the above issues, plate impact experiments were conducted on diamond single crystals along the [110] and [111] orientations to ∼120 GPa elastic impact stresses. Results for all three orientations, including the [100] orientation [14], are compared and discussed here. We point out that a previous study using laser shock compression examined the strength of type Ia and type IIa natural diamonds along different orientations [18]. However, as noted previously by Lang and Gupta [14], the experimental effort presented here differs significantly from that in Ref. [18] with regard to: determination of input stresses, shock wave loading methods and durations, experimental precision, and sample purity. Hence, it is difficult to compare the results from these two types of experiments except to comment on some observed trends, as we do in Sec. IV.

The present paper is organized as follows. The experimental method is summarized briefly in Sec. II, since it is similar to that described in Ref. [14]. Experimental results are presented and compared in Sec. III. Analysis of the experimental results are presented in Sec. IV, along with a discussion of the present and earlier studies. The main findings of this work are summarized in Sec. V.

II. EXPERIMENTAL METHOD

Type IIa natural diamond single crystals were obtained from Doubledee Harris Diamond Corp. and Element Six as transparent, optically polished plates. The plates were oriented to within 3° of the [110] or [111] directions, as verified using Laue x-ray diffraction. Figure 1 shows a schematic view of the plate impact experimental configuration. Similar to the experiments for the [100] orientation reported in Ref. [14], oxygen-free high conductivity (OFHC) copper disks were launched using a single-stage powder gun and a two-stage gun and were impacted onto a target assembly consisting of a diamond sample sandwiched between an OFHC copper buffer and a [100] oriented lithium fluoride optical window. The experimental parameters, including the measured impact velocities, are listed in Table I.

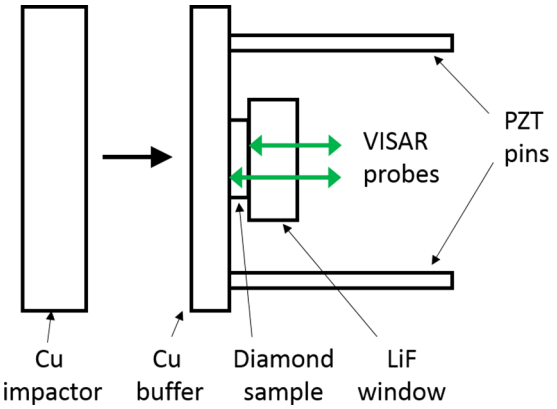

FIG. 1. Experimental configuration for measuring particle velocity profiles and shock wave velocity in shocked diamond single crystals.

Particle velocity histories were measured simultaneously at both interfaces of the diamond sample using a multipoint velocity interferometer system (VISAR) [19]. The VISAR probes were laterally separated by 0.75 mm at the diamond sample, as shown in Fig. 1. A dual velocity-per-fringe configuration was used to provide unambiguous fringe counts [20]. Four lead zirconate titanate (PZT) pins situated around the diamond samples (Fig. 1) provided a good measurement of the shock wave front tilt in each experiment. This information, together with the two VISAR profiles, was used to precisely determine the wave velocity through the diamond samples (rigorously, an average velocity over the sample thickness, as noted by one reviewer). The time duration of the experiments was governed by the arrival of release waves from the sample edges in the region of interest. Additional details regarding the experimental method can be seen in Ref. [21].

As shown elsewhere [22], pure longitudinal waves resulting in uniaxial strain can be propagated in cubic crystals shocked along [100], [110], and [111] orientations.

III. EXPERIMENTAL RESULTS

A total of eight plate impact experiments on diamond single crystals were carried out in this study: four on [110]-oriented samples and four on [111]-oriented samples. The diamond samples were shocked to three different elastic impact stresses (EIS): ∼60, ∼90, and ∼120 GPa. The actual elastic impact stress for each experiment was determined by impedance matching [23] using published Hugoniot data for copper [24],

TABLE I. Experimental parameters for diamond single crystals shocked along the [110] and [111] orientations.

Experiment number	Sample orientation	Sample thickness (mm)	Projectile velocity (mm/μs)
1 (10-608)	[110]	0.437	2.089
2 (10-2S08)	[110]	0.620	2.786
3 (10-2S16)	[110]	0.603	2.812
4 (10-2S04)	[110]	0.631	3.584
5 (10-611)	[111]	0.534	2.111
6 (10-2S18)	[111]	0.549	2.785
7 (10-2S10)	[111]	0.520	2.825
8 (10-2S09)	[111]	0.531	3.591

the measured second-order [25] and third-order [11] elastic constants of diamond, and the measured impact velocity.

Particle velocity histories for shocked [110]-oriented single crystals, measured at the diamond-LiF interface, are shown in Fig. 2. The measured wave profile at 62 GPa elastic impact stress shows a sharp single wave, characteristic of a completely elastic response. At 88 GPa, the wave profile shows the expected elastic jump, followed by a slow decrease to a lower value and a subsequent gradual increase. Despite some fluctuations, the measured wave profile at 121 GPa shows the following features: a sharper decrease (than the 88 GPa profile) following the elastic jump and a second wave with some structure. The particle velocity decrease following the elastic jump, observed at 88 and 121 GPa elastic impact stress, is characteristic of a time-dependent, inelastic response [26–28]. The elastic wave amplitude at 121 GPa is lower than that observed at 88 GPa, consistent with the result reported previously for shocked [100] diamond [14].

Figure 3 shows the particle velocity histories, measured at the diamond-LiF interface, for shocked [111]-oriented diamond single crystals. The measured profiles for all three elastic impact stresses differ significantly from the corresponding measured [110] profiles. The measured wave profile for [111] diamond shocked to 63 GPa elastic impact stress shows an extremely gradual decrease in particle velocity following the initial elastic jump. Despite some fluctuations, the wave profiles measured at 90 and 122 GPa elastic impact stress show the following features: considerably sharper decreases (than the 63 GPa profile) following the elastic jumps, followed by structured second waves; the 122 GPa experiment shows a pronounced two-step structure in the second wave. The particle velocity decreases following the elastic jumps and the structured second waves are characteristic features of time-dependent inelastic response [17,26–28]. Similar to the [110] results, the elastic wave amplitude at 122 GPa is lower than that at 90 GPa for the [111] orientation.

For comparison, representative particle velocity histories from previous experiments [14] on [100]-oriented diamond single crystals are shown in Fig. 4. The measured wave profile at 61 GPa shows a completely elastic response, similar to the [110] results. At 90 GPa, the wave profile reached the expected elastic impact stress and remained at that stress for a significant time duration before dropping rapidly due to the onset of time-dependent inelastic deformation. At 115 GPa, the wave profile shows a sharp decrease following the elastic jump and a structured second wave, representative of a time-dependent

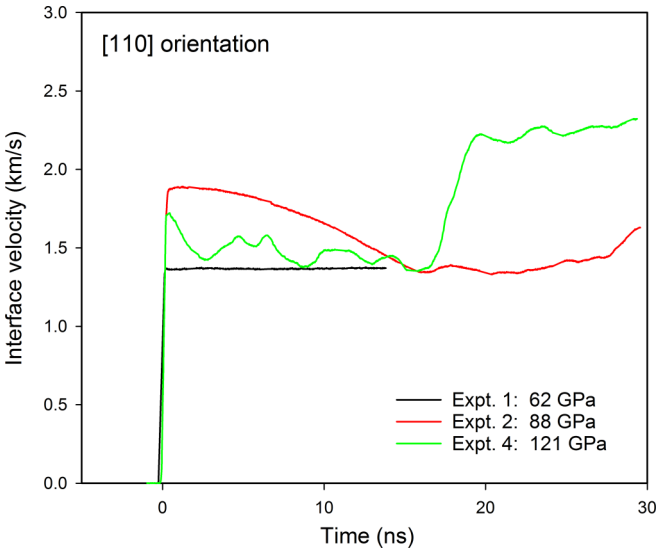

FIG. 2. Wave profiles, measured at the diamond/LiF interface, for diamond single crystals shocked along the [110] direction. The shock wave reaches the diamond-LiF interface at time $t = 0$.

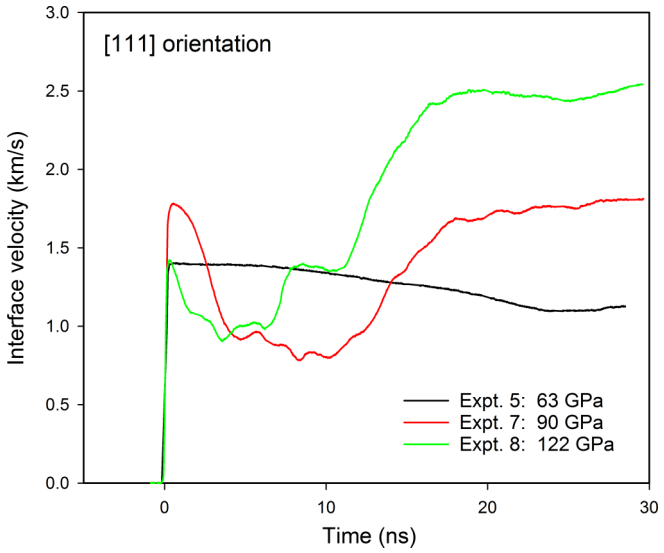

FIG. 3. Wave profiles, measured at the diamond/LiF interface, for diamond single crystals shocked along the [111] direction. The shock wave reaches the diamond-LiF interface at time $t = 0$.

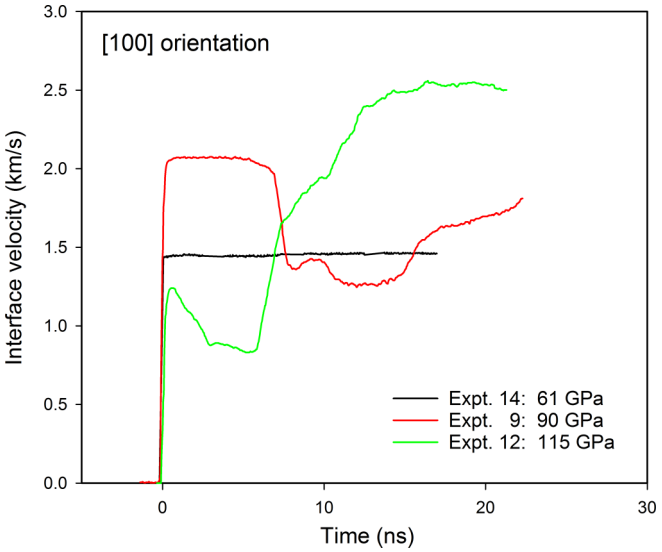

FIG. 4. Wave profiles, measured at the diamond/LiF interface, for diamond single crystals shocked along the [100] direction (from Refs. [14,21]). The shock wave reaches the diamond-LiF interface at time $t = 0$.

inelastic response [17,26–28]. Similar to the [110] and [111] results, the elastic wave amplitude for the wave profile at 115 GPa is lower than that for the 90 GPa profile, as noted previously [14].

To summarize, wave profile measurements for the three crystal orientations demonstrate the following features: significant dependence on crystal orientation; a sharp elastic jump; strongly time-dependent, inelastic response following the elastic wave; and in all cases, the elastic wave amplitude for ~120 GPa was lower than the elastic wave amplitude for ~90 GPa.

IV. ANALYSIS AND DISCUSSION

A. Elastic state characterization

The elastic shock wave velocity for each experiment was determined from the wave traversal time through the sample using the measured particle velocity histories at each interface of the diamond, together with the measured wave front tilt. Details of the analysis, including the various sources of uncertainty, were described previously [14]. The shock velocities for all eight experiments are listed in Table II. The uncertainty in the shock velocity was calculated from the uncertainties in the measured traversal time and the sample thickness using standard methods of uncertainty analysis [29].

Using jump conditions and impedance matching (as shown, for example, in Ref. [23]), the in-material particle velocity, longitudinal stress, and density at the peak of the elastic waves were determined from the measured elastic shock velocity, the measured elastic wave amplitude at the diamond-LiF interface, and the measured LiF Hugoniot [30]. Compared to Ref. [23], the present case is simpler since it involves elastic unloading in the diamond from the LiF; however, the analytic procedure is the same. The results for all eight experiments are listed in Table II. The uncertainties in the in-material particle velocities and stress amplitudes in Table II were estimated by varying the shock velocity and interface velocity values within their range of uncertainty and repeating the impedance matching calculations.

We emphasize that the use of jump conditions and impedance matching is rigorously correct for determining the in-material elastic wave states [26]. However, it is not valid for subsequent portions of the wave profile, due to the time-dependent inelastic deformation response observed beyond the elastic limit (Figs. 2–4). Therefore, the peak states reached in the experiments presented here were not determined and, instead, the elastic impact stress is used to compare results from different experiments.

To compare results for all three orientations, Table II also shows the in-material particle velocity, longitudinal stress, and density at the peak of the elastic wave, determined in previously reported experiments on shocked [100] diamond [14]. The results shown differ slightly from those in Ref. [14] due to a reanalysis of the previous measurements. Results are included from experiments on both natural (n) and synthetic (s) type IIa diamond single crystals. As shown previously [14], the elastic limits measured for natural and synthetic [100] diamond are comparable. Therefore, natural and synthetic diamond will not be distinguished in the subsequent discussion.

Figure 5 shows the elastic wave amplitudes (elastic limits) from Table II, as a function of the elastic impact stress, for all three crystal orientations. The results show that the elastic wave amplitudes reached the expected elastic impact stress in samples shocked to stresses less than 90 GPa. For experiments to ~90 GPa, some of the elastic wave amplitudes in [100] and [111] diamond did not fully attain the elastic impact stress. For experiments to ~120 GPa, the elastic wave amplitudes for all three orientations were considerably lower than the elastic impact stress. However, these amplitudes differed significantly for the three orientations, demonstrating a strong orientation dependence.

The lower elastic wave amplitudes observed for larger elastic impact stresses is somewhat surprising, based on the response expected for materials where the underlying inelastic deformation mechanism is plastic deformation due to dislocation motion. For example, wave profiles measured previously for shocked LiF single crystals showed larger elastic wave amplitudes for larger peak stresses [27].

B. Maximum resolved shear stress

As pointed out in previous studies on single crystals [15,16], the longitudinal stress achieved by the elastic wave is not a good measure of strength in shocked single crystals because the longitudinal and lateral stresses can vary significantly for different orientations due to crystalline anisotropy. Instead, resolved shear stresses (RSS) on relevant crystal planes are a better measure of strength. Therefore, to gain insight into the results presented here, the RSS on the commonly considered $\{111\}\langle 110\rangle$ slip systems [2–4,8,31] for diamond were determined for each experiment.

The RSS on the $\{111\}\langle 110\rangle$ slip systems are related to the longitudinal and lateral stresses using the following equations [15]:

TABLE II. Experimental results for diamond single crystals shocked along the [110] and [111] directions to elastic impact stress σ_{imp}. The measured elastic shock velocity $U_{s,\text{el}}$ is shown, together with the following in-material variables at the peak of the elastic wave: particle velocity u_p, density ρ, longitudinal stress σ_1', lateral stresses σ_2' and σ_3', resolved shear stress τ, and resolved normal stress σ_N on the $\{111\}\langle 110\rangle$ slip systems. Lateral stresses were calculated using the second-order [25] and third-order [11] elastic constants for diamond. For the [110] orientation, the two lateral stresses are not equivalent and two different resolved shear stresses arise on $\{111\}\langle 110\rangle$ slip systems; the τ shown is the larger of the two. Results for [100] diamond crystals from Refs. [14,21] are shown for comparison.

			Elastic wave						
Experiment-orientation-sample type[a]	σ_{imp} (GPa)	$U_{s,\text{el}}$ (km/s)	u_p (km/s)	ρ (g/cm^3)	σ_1' (GPa)	σ_2' (GPa)	σ_3' (GPa)	τ (GPa)	σ_N (GPa)
1[b]-[110]-n	61.9	20.40 ± 0.19	0.867 ± 0.011	3.671	62.1 ± 1.4	−0.11	3.95	23.7	42.7
2-[110]-n	88.0	20.42 ± 0.14	1.217 ± 0.012	3.738	87.4 ± 1.4	−0.78	4.80	33.7	59.9
3-[110]-n	89.1	20.21 ± 0.15	1.223 ± 0.012	3.741	86.9 ± 1.5	−0.81	4.83	33.5	59.5
4-[110]-n	121.0	20.54 ± 0.11	1.128 ± 0.011	3.719	81.5 ± 1.3	−0.55	4.61	31.4	55.9
5-[111]-n	62.9	19.93 ± 0.10	0.885 ± 0.011	3.678	62.0 ± 1.1	1.79		16.4	8.5
6-[111]-n	88.2	20.54 ± 0.22	1.207 ± 0.012	3.734	87.2 ± 1.8	2.06		23.2	11.5
7-[111]-n	89.8	20.49 ± 0.12	1.167 ± 0.011	3.727	84.0 ± 1.3	2.04		22.3	11.1
8-[111]-n	121.5	20.67 ± 0.17	0.951 ± 0.011	3.685	68.6 ± 1.4	1.84		18.2	9.3
9[c,d]-[100]-n	90.3	18.27 ± 0.09	1.368 ± 0.012	3.800	87.9 ± 1.2	13.3		30.5	38.1
10[c,d]-[100]-n	92.2	18.57 ± 0.12	1.388 ± 0.012	3.799	90.7 ± 1.4	13.2		31.6	39.0
11[c,d]-[100]-n	92.6	18.52 ± 0.11	1.313 ± 0.012	3.783	85.5 ± 1.3	12.3		29.9	36.7
12[c,d]-[100]-n	115.3	18.24 ± 0.15	0.849 ± 0.011	3.687	54.4 ± 1.2	7.31		19.2	23.0
13[c,d]-[100]-n	118.3	18.19 ± 0.14	0.829 ± 0.011	3.683	53.0 ± 1.1	7.11		18.7	22.4
14[b,d]-[100]-s	61.0	18.46 ± 0.11	0.941 ± 0.011	3.704	61.1 ± 1.1	8.15		21.6	25.8
15[b,d]-[100]-s	71.8	18.39 ± 0.11	1.098 ± 0.012	3.738	71.0 ± 1.2	9.89		24.9	30.3
16[c,d]-[100]-s	90.3	18.56 ± 0.12	1.338 ± 0.012	3.788	87.3 ± 1.3	12.6		30.5	37.5
17[c,d]-[100]-s	92.0[e]	18.42 ± 0.10	1.449 ± 0.012	3.815	93.9 ± 1.3[e]	14.1		32.6	40.7
18[c,d]-[100]-s	115.1	18.29 ± 0.11	0.917 ± 0.011	3.701	59.0 ± 1.1	8.00		20.8	25.0
19[c,d]-[100]-s	115.7	18.41 ± 0.19	0.847 ± 0.011	3.684	54.8 ± 1.3	7.16		19.4	23.0
20[c,d]-[100]-s	116.5	18.49 ± 0.17	0.939 ± 0.012	3.703	61.0 ± 1.3	8.10		21.6	25.7
21[c,d]-[100]-s	118.0	18.28 ± 0.17	0.917 ± 0.012	3.701	58.9 ± 1.3	8.00		20.8	25.0

[a]n and s indicate natural and synthetic type IIa diamond samples, respectively.
[b]A purely elastic response was observed in this experiment.
[c]Reference [14].
[d]Reference [21].
[e]The larger value of σ_1', compared to σ_{imp}, was attributed to experimental scatter in Ref. [14].

[100] orientation:

$$\tau = \frac{1}{\sqrt{6}}|\sigma'_{11} - \sigma'_{22}|, \tag{1}$$

[110] orientation:

$$\tau = \frac{1}{\sqrt{6}}|\sigma'_{11} - \sigma'_{33}|, \tag{2a}$$

$$\tau = \frac{1}{\sqrt{6}}|\sigma'_{22} - \sigma'_{33}|, \tag{2b}$$

[111] orientation:

$$\tau = \frac{\sqrt{2}}{3\sqrt{3}}|\sigma'_{11} - \sigma'_{22}|, \tag{3}$$

where the stress components shown above are expressed in a coordinate system that is aligned with the direction of shock compression for each crystal orientation [15]. To determine the RSS, the measured longitudinal stress was used in Eqs. (1)–(3), together with the lateral stresses determined using finite strain elasticity theory [32,33] and the measured second-order [25] and third-order [11] elastic constants of diamond. The lateral stresses and RSS determined for each experiment are also shown in Table II. For the [110] orientation, the two lateral stresses are not equivalent and the $\{111\}\langle 110\rangle$ slip systems can have one of two different nonzero RSS values. Only the larger of the two RSS values is considered here.

Figure 6 shows the RSS values from Table II as a function of the elastic impact stress (solid symbols). The solid curves are RSS values for uniaxial elastic compression along each orientation, calculated using the second-order [25] and third-order [11] elastic constants of diamond. For elastic impact stresses up to ∼90 GPa, the RSS values from Table II agree well with the calculated curves. At ∼120 GPa elastic impact stress, the resolved shear stresses for all three orientations are significantly lower, compared to their maximum values at ∼90 GPa, consistent with the drop in elastic wave amplitude shown in Fig. 5. The drop in resolved shear stress at the higher elastic impact stress suggests an orientation dependent reduction in strength, with the [100] orientation showing the largest reduction and the [110] orientation showing the smallest reduction.

The dashed curves shown in Fig. 6 are the RSS values calculated using the second-order elastic constants only (third-order elastic constants set to zero) to evaluate the role of third-

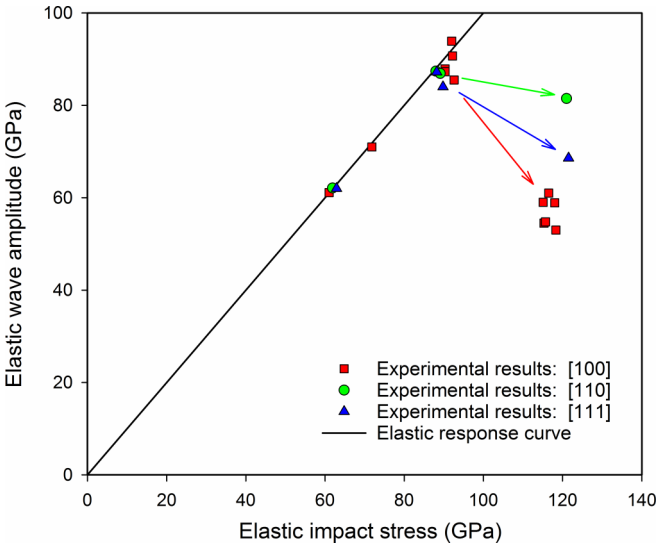

FIG. 5. Elastic wave stress amplitude versus elastic impact stress for shocked diamond single crystals. The symbols are experimental results from Table II. The black curve is the locus of shocked states for which the elastic wave amplitude reaches the expected elastic impact stress.

order constants. The solid and dashed curves differ somewhat, showing that the third-order elastic constants are important for an accurate description of shocked diamond. However, Fig. 6 also shows that our results and findings are not qualitatively affected by the presence or absence of the third-order elastic constants in our analysis.

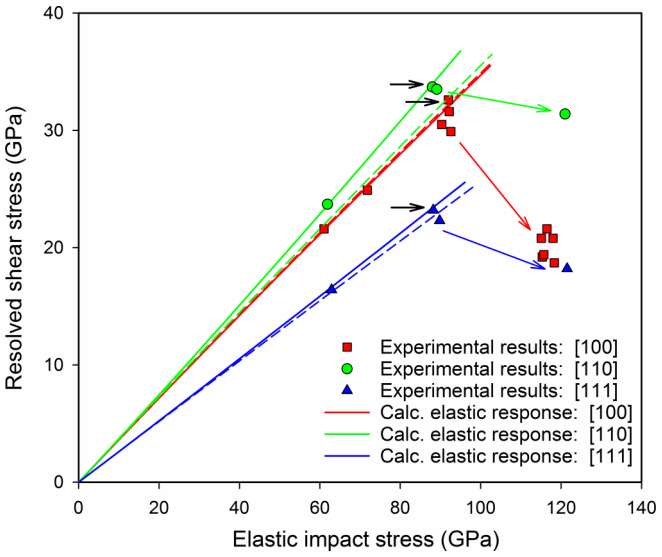

FIG. 6. Resolved shear stress for the $\{111\}\langle 110\rangle$ slip system as a function of elastic impact stress. The symbols are experimental results from Table II; the small horizontal arrows indicate the maximum resolved shear stress for each orientation. The solid curves were calculated using Eqs. (1)–(3), together with the second-order [25] and third-order [11] elastic constants of diamond. To show the effect of third-order elastic constants, the dashed curves were calculated using the second-order elastic constants only.

TABLE III. Maximum resolved shear stress (MRSS), ratio of MRSS to shear modulus, resolved normal stress (RNS), and ratio of MRSS to RNS for the $\{111\}\langle 110\rangle$ slip system of diamond shocked along different orientations.

Orientation	MRSS: τ_{max}(GPa)	$\frac{\tau_{max}}{G_{\{111\}}}$	RNS: σ^N(GPa)	$\frac{\tau_{max}}{\sigma^N}$
[100]	32.6	0.064	40.7	0.80
[110]	33.7	0.066	59.9	0.56
[111]	23.2	0.045	11.5	2.02

The elastic limit is quantified here using the maximum resolved shear stress (MRSS) on the $\{111\}\langle 110\rangle$ system τ_{max}, which is listed in Table III for each crystal orientation. Table III also shows the ratio of the MRSS to the shear modulus relevant for $\{111\}$ planes in diamond $\tau_{max}/G_{\{111\}}$, where $G_{\{111\}}$ is given (in the linear approximation) by

$$G_{\{111\}} = \tfrac{1}{3}(C_{11} - C_{12} + C_{44}) \quad (4)$$

and C_{ij} are the second-order elastic constants [25]. The elastic limits listed in Table III show strong orientation dependence: the MRSS value for the [111] orientation ($\tau_{max} \approx G_{\{111\}}/20$) is significantly smaller compared to that observed for the [100] and [110] orientations ($\tau_{max} \approx G_{\{111\}}/15$), showing that the wave propagation direction relative to the slip system is an important factor for determining the strength of shocked diamond single crystals.

The measured MRSS values in this work are smaller than the calculated theoretical shear strength ($\sim G_{\{111\}}/4$) for the $\{111\}\langle 110\rangle$ system in perfect diamond single crystals [3,4,8]. As is well known, defects in real crystals typically lead to the onset of inelastic deformation at lower resolved shear stresses, resulting in lower strength, compared to perfect crystals [34,35].

C. Role of normal stress

Previous theoretical calculations for diamond under different loading conditions have suggested that the stress component normal to the slip plane can significantly affect the calculated shear strength [36–38]. Therefore, to better understand the orientation dependence of the MRSS (Table III), the RSS value determined for each experiment is shown in Fig. 7 as a function of the stress component normal to the $\{111\}$ planes or the resolved normal stress (RNS). The RNS values were determined from the longitudinal and lateral stresses in Table II using the following equations:

[100] orientation:

$$\sigma_N = \tfrac{1}{3}|\sigma'_{11} + 2\sigma'_{22}|, \quad (5)$$

[110] orientation:

$$\sigma_N = \tfrac{1}{3}|2\sigma'_{11} + \sigma'_{33}|, \quad (6)$$

[111] orientation:

$$\sigma_N = \tfrac{1}{9}|\sigma'_{11} + 8\sigma'_{22}|. \quad (7)$$

In addition, RSS and RNS values, calculated for uniaxial elastic compression along each orientation, are shown in Fig. 7 (solid curves) and excellent agreement is observed with the experimental results. The slopes (in the linear approximation)

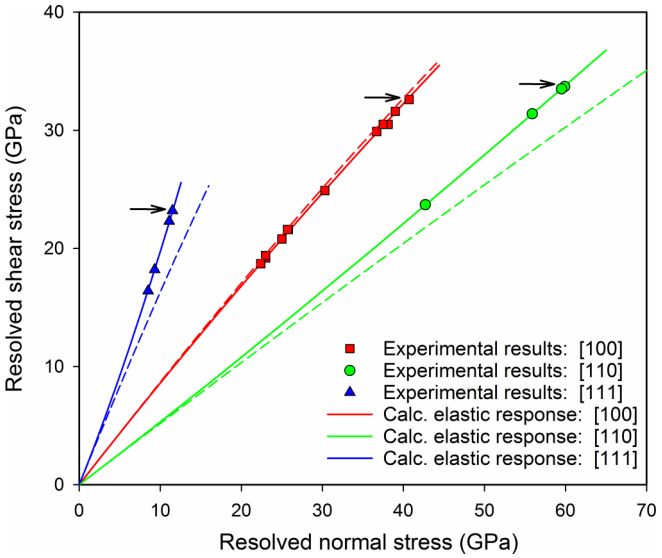

FIG. 7. Resolved shear stress as a function of resolved normal stress for the {111}⟨110⟩ slip system. The symbols are experimental results from Table II; the arrows indicate the maximum resolved shear stress for each orientation. The curves were calculated using Eqs. (1)–(3), together with the second-order [25] and third-order [11] elastic constants of diamond. To show the effect of third-order elastic constants, the dashed curves were calculated using the second-order elastic constants only.

of the three curves in Fig. 7 give the ratio of the RSS to the RNS for each orientation; these ratios are listed in Table III. The largest ratio (corresponding to the smallest RNS value for a given RSS value) is associated with the [111] orientation, which is the orientation that showed the smallest MRSS value. Conversely, the smallest ratio (corresponding to the largest RNS value for a given RSS value) is associated with the [110] orientation, which is the orientation that showed the largest MRSS value. Thus, the results shown in Fig. 7 demonstrate that the MRSS values attained are strongly dependent on the corresponding RNS values, and this dependence explains the observed anisotropic strength of shocked diamond single crystals: [110] > [100] > [111]. That is, the magnitude of the stress component normal to the slip plane plays a key role in inhibiting the onset of inelastic deformation in diamond single crystals.

The present results lead to two key findings: the elastic limit (or material strength) of diamond—a very strong, brittle, anisotropic solid—cannot be described using traditional isotropic approaches (e.g. Ref. [6]); and typical metal plasticity models based on dislocation slip (e.g., Refs. [39,40]) cannot be used to describe the inelastic deformation of diamond because they do not incorporate the normal stress dependence.

D. Inelastic response

As mentioned in Sec. III, the measured wave profiles in Figs. 2–4 show a strongly time-dependent inelastic deformation response. However, understanding the specific mechanism(s) underlying the time-dependent inelastic response is challenging. Although the measured wave profiles beyond the elastic limit contain significant and useful information regarding the inelastic deformation response, the time-dependent response seen in Figs. 2–4 precludes an impedance matching analysis beyond the elastic limit [26]. Rigorous analysis of the complete wave profiles, including characterization of the peak state, requires numerical simulations that incorporate a continuum description of time-dependent, anisotropic, inelastic deformation in shocked diamond single crystals. Because such a material description is not currently available, development of the same is an important need.

The lower resolved shear stress at ∼120 GPa elastic impact stress (Fig. 6) compared to the resolved shear stress at ∼90 GPa elastic impact stress and the effect of stress normal to the slip planes (Fig. 7) are not consistent with typical dislocation slip mechanisms of inelastic deformation [27,39,40]. Instead, these results suggest that alternative inelastic deformation mechanisms play an important role in shocked diamond single crystals. For strong solids such as diamond, the alternative mechanisms are likely those characteristic of a time-dependent, brittle response, such as the development of shear cracks [41] or adiabatic shear bands [42]. Further work is needed to develop and examine the applicability of such models for shock compression of diamond.

E. Comparison with laser-shock experiments

As noted in Sec. I, the experimental effort presented here differs significantly from the laser-shock experiments reported in Ref. [18] with regard to: determination of input stresses, loading methods and durations, experimental precision, and sample purity. Furthermore, except for the lowest stress, the peak stresses (100–1000 GPa) inferred in Ref. [18] are significantly higher than the elastic impact stresses examined here.

Regarding analysis of the measured wave profiles, the time-independent approach (impedance matching) used in Ref. [18] is not correct beyond the elastic limit due to the observed time-dependent inelastic deformation response of diamond, similar to that presented here. For this reason, and because of the loading conditions used, determination of the peak states reported in Ref. [18] remains an open question. The strength values for shocked diamond single crystals, reported in Ref. [18], were determined using an analysis approach developed to describe time-independent metal plasticity [43]. Because this approach involves the implicit assumption of an isotropic elastic-plastic response, it is not correct for single crystals. We also note that, although resolved shear stresses for shocked diamond single crystals were calculated in Ref. [18], they were not reported for the {111}⟨110⟩ slip system considered here.

Because of the above significant differences, it is difficult to compare the results presented here with those from Ref. [18] except for a few qualitative comments. Overall, the elastic wave amplitudes reported in Ref. [18] are somewhat smaller than, but comparable to, those presented here. Likewise, the limited resolved shear stress determinations presented in Ref. [18] for the {111}⟨112⟩ slip system suggest that the corresponding resolved shear stresses on the {111}⟨110⟩ slip system are likely comparable to the maximum resolved shear stresses presented in Table III. However, the lower elastic limit at higher elastic input stress, presented here, is markedly different from the trend reported in Ref. [18].

V. SUMMARY AND CONCLUSIONS

To address longstanding questions regarding the effect of crystalline anisotropy on the elastic limit or material strength of diamond single crystals, plane shock wave experiments were conducted on diamond samples. Wave profiles were measured for [110]- and [111]-oriented diamond single crystals shocked to elastic impact stresses as high as ∼120 GPa. The results were compared with similar measurements published previously for shock compression along the [100] direction [14]. The main findings from our work are summarized below.

(1) Wave profiles for all three orientations showed large elastic wave amplitudes followed by strongly time-dependent inelastic deformation.

(2) From the measured wave profiles, the elastic limits—determined under well characterized uniaxial strain loading conditions—showed a significant orientation dependence.

(3) For all three orientations, smaller elastic wave amplitudes were observed at ∼120 GPa elastic impact stress, compared to those at ∼90 GPa. As pointed out previously [14], smaller elastic limits for larger peak stresses are surprising and further work is required to understand this result.

(4) Resolved shear stresses were calculated for the $\{111\}\langle 110\rangle$ slip systems of diamond. The maximum resolved shear stress (MRSS) for the different orientations revealed significant orientation dependence: The MRSS values are largest ($\tau_{max} \sim G/15$) for the [110] and [100] orientations and smallest ($\tau_{max} \sim G/20$) for the [111] orientation. The MRSS values determined for the [110] and [100] orientations correspond to 25%–30% of the calculated theoretical shear strength for $\{111\}\langle 110\rangle$ slip systems in perfect diamond single crystals [3,4,8].

(5) The MRSS values depend strongly on the stress component normal to the $\{111\}$ slip planes (or the resolved normal stress), providing an explanation for the observed orientation dependence of strength in shocked diamond single crystals: [110] > [100] > [111]. The results show that the resolved normal stress plays a key role in inhibiting the onset of inelastic deformation in shocked diamond single crystals.

(6) The lower elastic wave amplitudes at larger impact stresses and the effect of stress normal to the slip planes observed here are not consistent with typical dislocation slip mechanisms [27,39,40]. Instead, our results suggest a strongly time-dependent inelastic deformation response that is characteristic of shocked brittle solids [41,42].

(7) The present results show that the elastic limit (or material strength) of shocked diamond single crystals cannot be described using traditional isotropic approaches (e.g., Ref. [6]). In addition, typical metal plasticity models (e.g., Refs. [18,43]) cannot be used to describe the inelastic deformation of shocked diamond single crystals.

The present work has provided important insights into the elastic-inelastic response of shocked diamond single crystals, including the effect of crystalline anisotropy on the elastic limit. However, rigorous analysis of the inelastic deformation response beyond the elastic limit, including characterization of the peak state, requires numerical simulations that incorporate a time-dependent, anisotropic, material model for shocked diamond. Therefore, development of the same is an important need.

In previous studies, solids shocked to high stresses (approximately one half of the melt stress or greater) have often been modeled using the hydrodynamic approximation (no material strength). In particular, the hydrodynamic approximation was used by Knudson *et al.* in their work on polycrystalline diamond shocked to stresses of 550 GPa and above [44]. In view of the previous work [44], the results presented here raise the following question: At what stresses does the hydrodynamic response become a good approximation for shocked diamond single crystals? A careful experimental study of diamond single crystals subjected to plate impact loading to high stresses and the development of appropriate material models are required to address this important question.

ACKNOWLEDGMENTS

N. Arganbright, C. Bakeman, L. Jones, K. Perkins, Y. Toyoda, and K. Zimmerman are sincerely thanked for their help with the impact experiments. This work was supported by the Department of Energy/NNSA under Cooperative Agreement No. DE-NA0000970 and No. DE-NA0002007.

[1] J. E. Field, *The Properties of Natural and Synthetic Diamond* (Academic, New York, 1992).
[2] T. Evans and R. K. Wild, Philos. Mag. **12**, 479 (1965).
[3] W. R. Tyson, Philos. Mag. **14**, 925 (1966).
[4] A. Kelly, W. R. Tyson, and A. H. Cottrell, Philos. Mag. **15**, 567 (1967).
[5] A. L. Ruoff, in *High Pressure Science and Technology*, edited by K. D. Timmerhaus and M. S. Barber (Plenum, New York, 1979), pp. 525–548.
[6] A. L. Ruoff and H. Luo, J. Appl. Phys. **70**, 2066 (1991).
[7] D. Roundy and M. L. Cohen, Phys. Rev. B **64**, 212103 (2001).
[8] S. Ogata, J. Li, N. Hirosaki, Y. Shibutani, and S. Yip, Phys. Rev. B **70**, 104104 (2004).
[9] M. I. Eremets, I. A. Trojan, P. Gwaze, J. Huth, R. Boehler, and V. D. Blank, Appl. Phys. Lett. **87**, 141902 (2005).
[10] J. M. Lang and Y. M. Gupta, Phys. Rev. Lett. **106**, 125502 (2011).
[11] J. M. Winey, A. Hmiel, and Y. M. Gupta, J. Phys. Chem. Solids **93**, 118 (2016).
[12] K. Kondo and T. J. Ahrens, Geophys. Res. Lett. **10**, 281 (1983).
[13] M. D. Knudson, J. R. Asay, S. C. Jones, and Y. M. Gupta, Sandia National Laboratories Report No. SAND2001-3838, 2001.
[14] J. M. Lang and Y. M. Gupta, J. Appl. Phys. **107**, 113538 (2010).
[15] J. N. Johnson, O. E. Jones, and T. E. Michaels, J. Appl. Phys. **41**, 2330 (1970).
[16] Y. M. Gupta, J. Appl. Phys. **48**, 5067 (1977).
[17] L. E. Pope and J. N. Johnson, J. Appl. Phys. **46**, 720 (1975).
[18] R. S. McWilliams, J. H. Eggert, D. G. Hicks, D. K. Bradley, P. M. Celliers, D. K. Spaulding, T. R. Boehly, G. W. Collins, and R. Jeanloz, Phys. Rev. B **81**, 014111 (2010).

[19] L. M. Barker and R. E. Hollenbach, J. Appl. Phys. **43**, 4669 (1972).
[20] D. H. Dolan, Sandia National Laboratories Report No. SAND2006-1950, 2006.
[21] J. M. Lang, Ph.D. Dissertation, Washington State University, 2013.
[22] J. M. Winey and Y. M. Gupta, J. Appl. Phys. **96**, 1993 (2004).
[23] S. J. Turneaure, J. M. Winey, and Y. M. Gupta, J. Appl. Phys. **100**, 063522 (2006).
[24] A. C. Mitchell and W. J. Nellis, J. Appl. Phys. **52**, 3363 (1981).
[25] H. J. McSkimin and P. Andreatch, Jr., J. Appl. Phys. **43**, 2944 (1972).
[26] J. R. Asay, G. R. Fowles, G. E. Duvall, M. H. Miles, and R. F. Tinder, J. Appl. Phys. **43**, 2132 (1972).
[27] Y. M. Gupta, J. Appl. Phys. **46**, 3395 (1975).
[28] Y. M. Gupta, G. E. Duvall, and G. R. Fowles, J. Appl. Phys. **46**, 532 (1975).
[29] J. R. Taylor, *An Introduction to Error Analysis*, 2nd ed. (University Science Books, California, 1982), p. 75.
[30] W. J. Carter, High Temp. -High Press. **5**, 313 (1973).
[31] N. S. Brar and W. R. Tyson, Scripta Metal. **6**, 587 (1972).
[32] D. C. Wallace, in *Solid State Physics*, edited by H. Ehrenreich, F. Seitz, and D. Turnbull (Academic, New York, 1970), Vol. 25, p. 301.
[33] R. N. Thurston, in *Physical Acoustics: Principles and Methods*, edited by W. P. Mason (Academic, New York, 1964), Vol. 1, Part A, p. 1.
[34] A. H. Cottrell, *Dislocations and Plastic Flow in Crystals* (Clarendon, Oxford, 1953).
[35] A. Kelly and N. H. MacMillan, *Strong Solids* (Clarendon, Oxford, 1986).
[36] Y. Umeno and M. Černý, Phys. Rev. B **77**, 100101(R) (2008).
[37] Y. Umeno, Y. Shiihara, and N. Yoshikawa, J. Phys. Condens. Matter **23**, 385401 (2011).
[38] H. Chacham and L. Kleinman, Phys. Rev. Lett. **85**, 4904 (2000).
[39] J. P. Hirth and J. Lothe, *Theory of Dislocations* (McGraw-Hill, New York, 1968).
[40] J. J. Gilman, *Micromechanics of Flow in Solids* (McGraw-Hill, New York, 1969), p. 76.
[41] B. Lawn, *Fracture of Brittle Solids* (Cambridge Press, Cambridge, 1993).
[42] T. W. Wright, *Physics and Mathematics of Adiabatic Shear Bands* (Cambridge University Press, Cambridge, 2002).
[43] G. R. Fowles, J. Appl. Phys. **32**, 1475 (1961).
[44] M. D. Knudson, M. P. Desjarlais, and D. H. Dolan, Science **322**, 1822 (2008).